

# Non-Reciprocal Wave Transmission in a Bilinear Spring-Mass System

Zhaocheng Lu<sup>1</sup>

Department of Mechanical and Aerospace  
Engineering,  
Rutgers University,  
Piscataway, NJ 08854-8058  
e-mail: zhaocheng.lu@rutgers.edu

Andrew N. Norris

Professor  
Department of Mechanical and Aerospace  
Engineering,  
Rutgers University,  
Piscataway, NJ 08854-8058  
e-mail: norris@rutgers.edu

*Significant amplitude-independent and passive non-reciprocal wave motion can be achieved in a one-dimensional (1D) discrete chain of masses and springs with bilinear elastic stiffness. Some fundamental asymmetric spatial modulations of the bilinear spring stiffness are first examined for their non-reciprocal properties. These are combined as building blocks into more complex configurations with the objective of maximizing non-reciprocal wave behavior. The non-reciprocal property is demonstrated by the significant difference between the transmitted pulse displacement amplitudes and energies for incidence from opposite directions. Extreme non-reciprocity is realized when almost-zero transmission is achieved for the propagation from one direction with a noticeable transmitted pulse for incidence from the other. These models provide the basis for a class of simple 1D non-reciprocal designs and can serve as the building blocks for more complex and higher dimensional non-reciprocal wave systems. [DOI: 10.1115/1.4045501]*

**Keywords:** non-linear vibration, vibration isolation, non-reciprocity, bilinear stiffness, one-way propagation, passive, amplitude-independent

## 1 Introduction

Reciprocity is a fundamental physical principle of wave motion which requires symmetry in wave transmission between any two points. The same incident wave traveling in opposite directions should result in the same transmitted wave. Recent advances have shown that the principle of reciprocity can be violated under special conditions in electromagnetism [1], acoustics [2–10], and other physical systems supporting wave propagation [11]. The ability to violate reciprocity in a controlled and passive manner opens the possibility of extreme wave dynamics and control mechanisms such as one-way propagation, acoustic diodes, etc. and provide revolutionary solutions to existing problems and useful tools for promising applications. The focus of the present work is breaking reciprocity of elastic waves using bilinear material properties.

There are several ways to break dynamic reciprocity. One is to remove time-reversal symmetry. For instance, gyroscopic inertial effects are used to break the time-reversal symmetry in a one-way phononic waveguide [2]. Spatiotemporal modulation of density and elastic properties provides another way to violate reciprocity. The direct modulation of elastic moduli and mass density simultaneously in both space and time introduces non-reciprocity due to the tilting of dispersion bands [3,4]. Non-reciprocal elastic wave propagation can be achieved via modulated stiffness realized by applying a wavelike deformation that alters the effective on-site stiffness [11]. A third way is using nonlinearity, which unlike the previous active examples provides a passive method to achieve non-reciprocity. Usually, the non-reciprocal phenomenon can be obtained by combining the nonlinearity with other assistant properties. In the acoustical domain, an acoustic diode can be achieved by utilizing the second-harmonic generation property of the nonlinear medium and the frequency selectivity of the sonic crystal [5,6]. Nonlinear acoustic non-reciprocity is also reported theoretically and experimentally in lattice structures incorporating strong stiffness nonlinearities, internal scale hierarchy, and asymmetry in their unit cell designs [7–9]. Weak nonlinearity can be used in

band gap manipulation which in turn leads to non-reciprocal behavior [10].

Bilinear springs present a unique case of nonlinearity, consisting of two different linear load-deformation relations. Unlike other nonlinearities, such as cubic [12,13], the bilinear relation is amplitude-independent; the nonlinearity enters only through the sign of the displacement. The analogous phenomenon in continuum mechanics occurs in materials with bilinear (also known as hetero-modular or bimodular) constitutive elastic behavior, which have been proposed as nonlinear models for studying contact forces [14], elastic solids containing cracks [15], and for the dynamics of geophysical systems, including granular media [16]. The discontinuity of the piecewise linear relation gives rise to a strong nonlinearity, for which it is difficult to find analytical solutions for simple wave problems. Wave motion in bimodular media has been studied extensively [17–26]. Even a small difference between the moduli in tension and compression immediately causes the appearance of shock waves [22]; however, linear viscosity eliminates the shocks. A good review of the literature of wave motion in continuous bimodular media, particularly the considerable work done by Russian researchers, can be found in Ref. [22], while Ref. [27] provides an earlier review. There are far fewer studies of wave motion in discrete spring-mass chains with bilinear spring forces. Of particular interest is the study [16] which analyzed impulse harmonic wave propagation in a 1D system of bilinear oscillators. Although they did not emphasize non-reciprocal effects, the authors noticed that sign inversion of a signal can be obtained, from tension to compression, that can lead to pulse spreading or shortening and possible shock formation. However, none of these prior studies of either continuous or discrete systems considered spatial inhomogeneity and asymmetry, which are necessary for producing non-reciprocal wave motion in the presence of material nonlinearity.

Here, we leverage the bilinear property to break wave reciprocity in a simple mechanical structure. Specifically, we consider a 1D bilinear spring-mass chain system in which the spatial modulation of bilinear stiffness is carefully investigated and designed. Incident pulses, generated by an external harmonic loading, are used to study transmitted pulse amplitudes and energies for incidence from opposite directions in the modulated chain. The non-reciprocal property of the system is demonstrated by the significant difference between the transmitted wave amplitudes from opposite directions and their energies. Zero transmission can be approximately achieved

<sup>1</sup>Corresponding author.

Contributed by the Technical Committee on Vibration and Sound of ASME for publication in the JOURNAL OF VIBRATION AND ACOUSTICS. Manuscript received July 25, 2019; final manuscript received November 14, 2019; published online November 20, 2019. Assoc. Editor: Stefano Gonella.

when the absolute amplitude ratio and energy ratio of the transmitted and incident pulse are both small enough. One-way propagation can be realized if almost-zero transmission is achieved for the propagation from one direction with a noticeable transmitted pulse from the other. The final non-reciprocal structure is obtained after careful design of the inhomogeneous and asymmetric spatial modulation of the stiffness and will be shown to display significant amplitude-independent non-reciprocity in a passive system. This simple 1D design could be the building block for complex, multiple dimensional non-reciprocal wave systems.

The paper is organized as follows: a 1D bilinear spring-mass chain system is introduced and the governing equations are discussed in Sec. 2. Some fundamental spatial modulations of the bilinear stiffness are presented and investigated in Sec. 3. Two non-reciprocal models are designed and demonstrated in Sec. 4. Section 5 concludes the paper.

## 2 One-Dimensional Bilinear Chain Overview

Consider a spring-mass chain system consisting of a linear part sandwiching a bilinear region as shown in Fig. 1. The bilinear section is a chain of identical masses, weak dampers, and bilinear springs with possible spatially dependent stiffness. The linear section consists of two chains of identical masses and uniform linear springs attached to both ends of the bilinear chain. An external loading is applied to generate the incident pulse in the linear chain. A perfectly matched layer (PML) is added to each end of the test chain (labeled chain in Fig. 1) in order to eliminate reflections, and hence the bilinear chain lies between two effectively semi-infinite linear chains. The PML is itself a chain of damped oscillators with damping coefficients that are incrementally “ramped-up” to prevent internal reflections [12].

The governing equations of the test chain system can be found by concentrating on the  $j$ th mass and its nearest neighbors, as shown by the central box in Fig. 1. The index  $j$ , which starts from 1 at the beginning of the test chain, also represents the  $j$ th spring  $K_j$  or damper  $C_j$ . Suppose that the number of masses in the linear part is  $2N_l$  and the number of masses in the bilinear part is  $N_{bl}$ . The total number of identical masses in this test chain is  $N = 2N_l + N_{bl}$ . Therefore, the number of the linear springs is  $2(N_l + 1)$  and the number of the bilinear springs is  $N_{bl} - 1$ . The total number of all springs is  $N + 1$ . The equation of motion for the  $j$ th mass is as follows:

$$M \ddot{U}_j - [K_{j+1}(U_{j+1} - U_j) + K_j(U_{j-1} - U_j)] - [C_{j+1}(\dot{U}_{j+1} - \dot{U}_j) + C_j(\dot{U}_{j-1} - \dot{U}_j)] = F \delta_{j1}, \quad j = 1, \dots, N \quad (1)$$

A pulse is used for the investigation of non-reciprocal properties [16]. The specific pulse adopted here is generated by an external harmonic loading of the form  $F = \pm F_0 \mathcal{H}(T) \mathcal{H}(2\pi/\Omega - T) \sin \Omega T$ , where  $F_0 > 0$  is the forcing amplitude and  $\Omega$  is the excitation frequency. The positive sign results in an incident pulse with compression followed by tension, called a compression–tension (CT) pulse (see Fig. 2). Conversely, the negative sign produces a tension–compression (TC) type of pulse.

We rewrite the equation of motion (Eq. (1)) in terms of dimensionless displacement  $u$  and time  $t$

$$u = \frac{U}{L}, \quad t = \Omega_0 T \quad (2)$$

where  $\Omega_0 = \sqrt{K_0/M}$  is the basic frequency and  $K_0$  is the linear stiffness. The dimensionless form of Eq. (1) is

$$u_j'' - [\kappa_{j+1}(u_{j+1} - u_j) + \kappa_j(u_{j-1} - u_j)] - [\zeta_{j+1}(u_{j+1}' - u_j') + \zeta_j(u_{j-1}' - u_j')] = f \delta_{j1}, \quad j = 1, \dots, N \quad (3)$$

where  $u'$  and  $u''$  denote the derivatives with respect to dimensionless time  $t$ , and the dimensionless stiffness and damping coefficients are

$$\kappa_j = \frac{K_j}{K_0}, \quad \zeta_j = \frac{C_j}{\sqrt{MK_0}} \quad (4)$$

and the dimensionless external forcing is

$$f = \pm f_0 \mathcal{H}(t) \mathcal{H}\left(\frac{2\pi}{\omega} - t\right) \sin \omega t \quad (5)$$

with  $f_0 = F_0/(L K_0)$  and  $\omega = \Omega/\Omega_0$ . Both the dimensionless stiffness  $\kappa_j$  and the dimensionless damping coefficient  $\zeta_j$  depend on their location or the index  $j$ . In the linear sections, the index takes the values  $1 \leq j \leq N_l + 1$  or  $N_l + N_{bl} < j \leq N + 1$ , and in the bilinear middle section,  $N_l + 1 < j \leq N_l + N_{bl}$ . The stiffness is

$$\kappa_j = \begin{cases} 1 + \Delta_{j,c} & \text{if } u_j - u_{j-1} < 0 \\ 1 + \Delta_{j,t} & \text{if } u_j - u_{j-1} > 0 \\ 1 & \text{linear sections} \end{cases} \quad \text{bilinear section} \quad (6)$$

where  $\Delta_{j,c}$  and  $\Delta_{j,t}$  are the dimensionless compressive and tensile stiffness increment, respectively. In terms of the bilinear stiffness,  $\Delta_j = \Delta K_j/K_0$  with  $\Delta K_j$  assuming different values depending on whether the spring is in compression or tension. The damping coefficient is taken as

$$\zeta_j = \begin{cases} \zeta_0 & \text{bilinear section} \\ 0 & \text{linear sections} \end{cases} \quad (7)$$

where  $\zeta_0$  is the constant damping coefficient in the bilinear chain. Expressions for the stiffness and damping coefficient in the PML can be found in Appendix A. Damping is not included in the linear sections so that we can more clearly see the incident and transmitted waves. The weak dampers in the bilinear section do not significantly affect the transmission. However, a small amount of damping has a strong smoothing effect in the presence of discontinuities, such as eliminating those shock-like structures that can arise in bilinear media. Details of comparison with and without damping are included in Appendix B. In this paper, we choose to include sufficient damping such that the transmitted wave forms are smooth. This allows us to make quantitative comparisons between transmission for incidence from opposite directions.

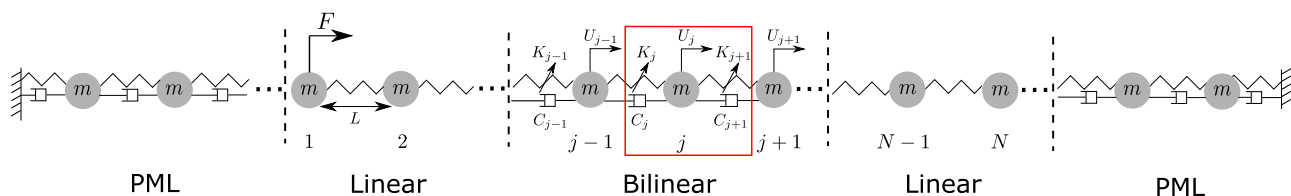


**Fig. 1** Schematic view of the 1D test chain system of identical masses with uniform linear springs and spatially varying bilinear springs. A PML is attached to each side of the test chain. An external force  $F$  is applied on the first mass in the linear chain on the left. The length  $L$ , assumed uniform, denotes the spacing between the equilibrium positions of two adjacent masses. Index  $j$  denotes the mass number, with identical masses  $m$  assumed. The box in the middle is the unit cell for equilibrium.  $U_j$  denotes the displacement of the  $j$ th mass;  $K_j$  and  $C_j$  denotes the  $j$ th spring and damper between  $j$ th and  $(j - 1)$ th mass, respectively.

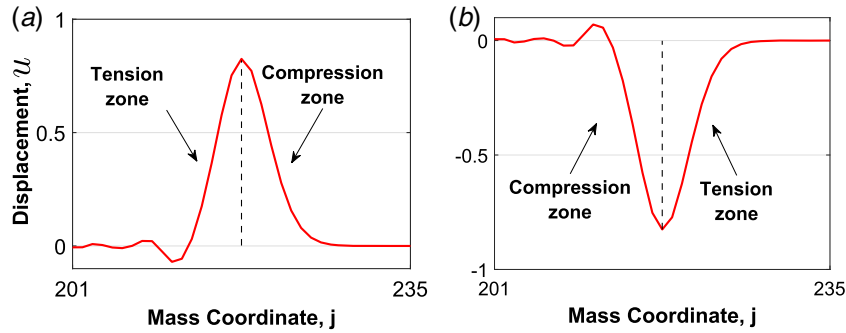


**Fig. 2** Incident pulses generated by an external forcing propagate in the linear chain and form the incident wave on the bilinear section. The dashed line divides the pulse into two different parts each of which contains springs in the same state, compression or tension. (a) CT pulse and (b) TC pulse.

The system of  $N$  linear and bilinear ordinary differential equations, Eq. (3), is solved numerically using ODE45 in MATLAB with time step  $\Delta t = 0.01$ .

### 3 Spatial Modulation of the Bilinear Stiffness

In this section, we explore the dynamic properties of several underlying spatial modulations of the bilinear stiffness in the test chain. The designs strictly follow the principle of spatial inhomogeneity and asymmetry which are critical for creating non-reciprocal propagation in the presence of nonlinearity.

A CT pulse, generated by setting a positive sign in the external forcing (Eq. (5)), is used to test the different modulations. As Fig. 2 depicts, the positive displacement corresponds to the movement of mass to the right and the negative to the left. Numerical results presented in this section are obtained using the parameters listed in Table 1.

We first assume that the stiffness of the bilinear spring is greater in compression than in tension. For simplicity, we set the stiffness in tension equal to the linear stiffness. Therefore,  $\Delta_{j,c} > \Delta_{j,t} = 0$ . Suppose that the increment  $\Delta_{j,c}$  can be either linearly increasing or decreasing over location with non-dimensional stiffness ranging in values between 1 and 2. For the linearly increasing modulation with  $N_l + 1 < j \leq N_l + N_{bl}$ , we have

$$\Delta_{j,c} = \frac{j - N_l - 1}{N_{bl} - 1} \quad (8)$$

and for the linearly decreasing modulation

$$\Delta_{j,c} = \frac{N_l + N_{bl} + 1 - j}{N_{bl} - 1} \quad (9)$$

Figures 3(a) and 3(b) depict the stiffness modulations of Eqs. (8) and (9), respectively.

Figures 3(c) and 3(d) show the displacement fields along the test chain at four different moments  $t_n = n t_1$  ( $n = 1, 2, 3, 4$ ) where  $t_1 = 44$  for modulations Figs. 3(a) and 3(b), respectively. The incident pulse propagates from left to right. Since a compressive wave travels with a higher speed than a tensile one in the bilinear

chain, we expect an increase in the distance between compressive and tensile zones with time for both modulations. A zero deformation zone, which is the horizontal region with nearly constant positive displacement, clearly indicates that the gap between compressive and tensile wave fronts is increasing with time. This phenomenon always happens when a faster wave is followed by a slower one.

Note that Figs. 3(a) and 3(b) consider a stiffness modulation slope of  $1/100$  (maximum value of  $\Delta_{j,c}$ /number of bilinear springs) with the maximum  $\Delta_{j,c}$  equal to 1. By modifying the slope of the stiffness curve (increasing or decreasing the maximum value of  $\Delta_{j,c}$ ), we find that the length of the zero deformation regime changes. See details in Appendix C.

It is clear that the different modulations of the bilinear stiffness result in distinct propagation processes. The decreasing modulation (Fig. 3(b) and Eq. (9)) leads to a more effective increase in the distance between two zones than the increasing modulation (Fig. 3(a) and Eq. (8)) because it is evident that an almost-zero deformation zone appears between times  $t_1$  and  $t_2$  in Fig. 3(d). By contrast, in Fig. 3(c), a noticeable almost-zero deformation zone appears between  $t_2$  and  $t_3$ .

The modulations of Figs. 3(a) and 3(b) induce impedance discontinuities, which in turn cause reflections. The discontinuity for Fig. 3(a) is seen as the incident wave from the left exits the bilinear chain, and conversely the discontinuity for Fig. 3(b) occurs as the wave enters the bilinear section. Interestingly, the latter situation results in a larger transmitted displacement amplitude, and in both cases, the transmitted displacement amplitudes are only slightly different from the incident amplitude. It is difficult to quantify the effect of impedance discontinuities for linear-to-bilinear springs since the latter do not have a single impedance. Any model of reflectivity at such interfaces would necessarily depend upon the pulse shape; however, we do not pursue that question in this paper.

We now examine the case where the bilinear spring stiffness is greater in tension than in compression:  $\Delta_{j,t} > \Delta_{j,c} = 0$ . As before, two types of modulations are considered for  $N_l + 1 < j \leq N_l + N_{bl}$ : the linearly increasing modulation

$$\Delta_{j,t} = \frac{j - N_l - 1}{N_{bl} - 1} \quad (10)$$

and the linearly decreasing modulation

$$\Delta_{j,t} = \frac{N_l + N_{bl} + 1 - j}{N_{bl} - 1} \quad (11)$$

Figures 4(a) and 4(b) show the modulations of Eqs. (10) and (11), respectively.

Figures 4(c) and 4(d) depict the displacement fields for modulations Figs. 4(a) and 4(b), respectively. These modulations are of particular interest due to the fact that a slower wave speed is

**Table 1** Parameters for numerical experiments:  $N_{pml}$  is the number of mass in each PML;  $N_l$  and  $N_{bl}$  are the numbers of masses in different parts of the chain system, see Eqs. (6) and (7);  $\zeta_0$  is the dimensionless damping coefficient in Eq. (7); and  $f_0$  is the dimensionless force amplitude in Eq. (5)

$N_{pml}$	$N_l$	$N_{bl}$	$\zeta_0$	$f_0$	$\omega$
200	49	101	0.1	0.01	0.5

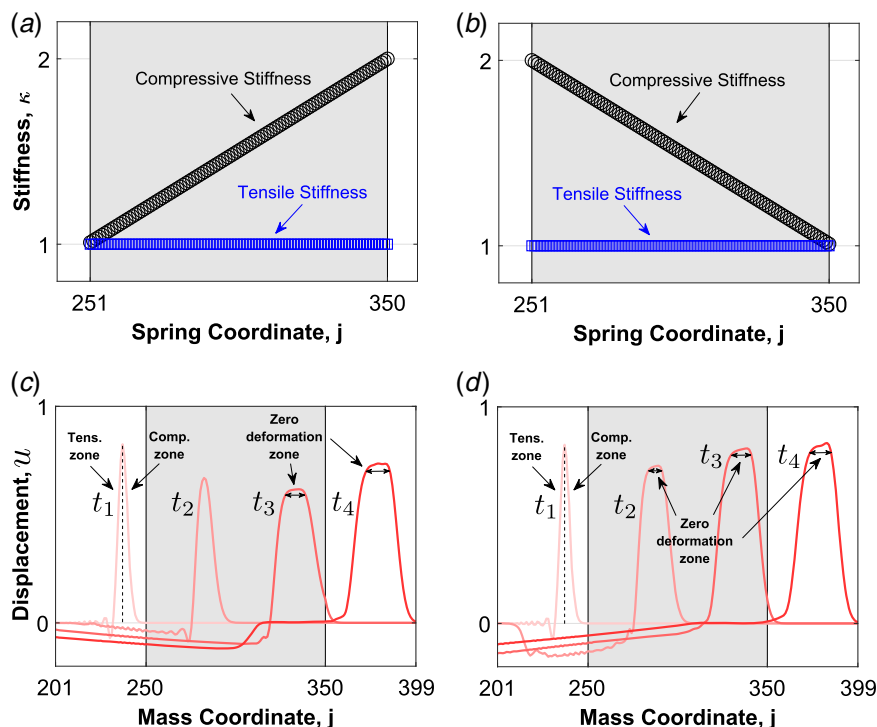


**Fig. 3** Dynamic properties of the bilinear spring chain with compressive stiffness varying linearly with position. The shaded region is the bilinear part of the test chain. (a) and (b) Two basic bilinear stiffness spatial modulations. (a) Linearly increasing compressive stiffness. (b) Linearly decreasing compressive stiffness. (c) and (d) Displacement fields at different moments for modulations (a) and (b), respectively.

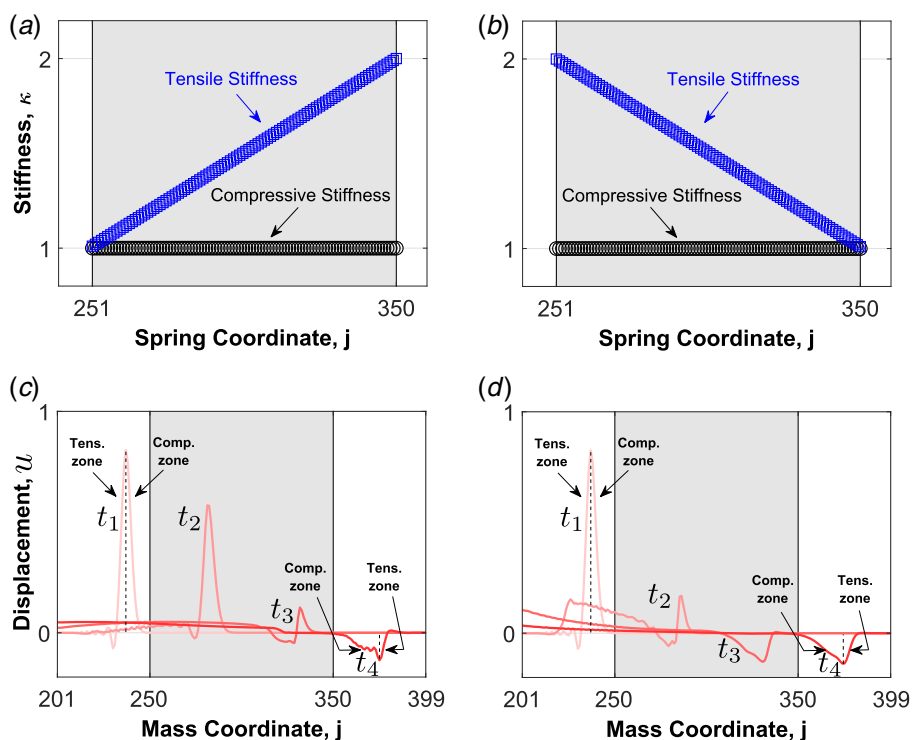


**Fig. 4** Dynamic properties of the bilinear spring chain with linearly varying tensile stiffness. The two basic spatial modulations of bilinear stiffness are shown in (a) linearly increasing tensile stiffness and (b) linearly decreasing tensile stiffness while (c) and (d) are the corresponding displacement fields of the test chain at different moments.



followed by a faster one in the bilinear chain. Consequently, the faster tensile wave front catches up with the slower compressive one, which makes a CT pulse change to TC one after transmission. This phenomenon of pulse-type change always happens when a slower wave is followed by a faster one. Similarly, we can observe distinct propagation processes for the different modulations. The linearly decreasing modulation (Fig. 4(b) and Eq. (11)) results in an effective change of pulse type that happens between times  $t_2$  and  $t_3$  in Fig. 4(d). However, for the other modulation (Fig. 4(a) and Eq. (10)), the change in pulse type takes place between  $t_3$  and  $t_4$  in Fig. 4(c).

Finally, we note the alternative TC incident pulse, which is generated by setting the negative sign in Eq. (5). Based on the previous findings, we expect (i) a change of pulse type for the modulations with the greater compressive stiffness and (ii) an increase in the distance between two zones for the modulations with the greater tensile stiffness. These expected dynamic properties are corroborated in Appendix C.

To sum up, the various spatial modulations of the bilinear stiffness investigated in this section can be used as the building blocks for more complex bilinear chain models with the potential of significant violation of wave reciprocity. This possibility is explored in the next section.

## 4 Non-Reciprocal Properties of the Bilinear Chain

**4.1 Two Non-Reciprocal Models.** Based on the findings in Sec. 3, we now design two spatially asymmetric and inhomogeneous models to break wave reciprocity. The bilinear chain in either model of Fig. 5 can be separated into two parts each of which is of the same form as one of the fundamental stiffness modulations discussed in Sec. 3. In the following discussions, blue and red arrows indicate the opposite pulse propagation directions in these models; blue for incidence from the left and red from the right.

We first define the models' parameters. For a pulse incident from the left, the section on the left-hand side of the dashed line is similar to the modulation in Fig. 3(b), but with different slope. The maximum difference between the compressive and tensile stiffness of the bilinear spring is  $a$ , and the total number of bilinear springs in this part is  $c$ . The section on the right is analogous to the modulation in Fig. 4(a) with the maximum stiffness difference  $b$  and the total bilinear springs number  $d$ . The index  $j$  takes the values  $N_l + 1 < j \leq N_l + 1 + c(N_{bl} - 1)/(c + d)$  for the section on the left and  $N_l + 1 + c(N_{bl} - 1)/(c + d) < j \leq N_l + N_{bl}$  on the right. Hence,

the dimensionless stiffness increments  $\Delta_{j,c}$  and  $\Delta_{j,t}$  can be expressed as

$$\Delta_{j,c} = \begin{cases} a \frac{N_l + 2 + \frac{c}{c+d}(N_{bl} - 1) - j}{\frac{c}{c+d}(N_{bl} - 1)} & \text{left section} \\ 0 & \text{right section} \end{cases} \quad (12)$$

$$\Delta_{j,t} = \begin{cases} 0 & \text{left section} \\ b \frac{j - N_l - 1 - \frac{c}{c+d}(N_{bl} - 1)}{\frac{d}{c+d}(N_{bl} - 1)} & \text{right section} \end{cases}$$

For pulse propagation from the right, the right-hand section is analogous to the modulation in Fig. 4(b) and the section on the left to the modulation in Fig. 3(a). The dimensionless stiffness increments follow accordingly; see Appendix D for details.

Our objective is that a CT pulse incident from the left produces a transmitted pulse with the same pulse type as the incident one and of comparable amplitude. Therefore, a long enough distance between the compression and tension zones is necessary in the left section. We introduce the linearly decreasing modulation in this section. If we set  $a$  small but  $c$  large as model I in Fig. 5(a) shows, the effect of the other section on the right is consequently weak because of the linearly increasing modulation and the small value of  $d$ . For model I, we have  $a < b$  and  $c > d$ . Alternatively, we set  $a$  large but  $c$  small in the left section for model II depicted in Fig. 5(b), and consequently the effect of the other section is weak because of the linearly increasing modulation and the small value of  $b$ . We have  $a > b$  and  $c < d$  for model II. When the same CT pulse is incident from the right, we require that the catch-up phenomenon takes place sequentially in each section to gradually minimize the pulse amplitude. In order to ensure the change in pulse type in the section on the right, we apply the linearly decreasing modulation in that region. We can either set  $b$  large and  $d$  small as model I in Fig. 5(a) shows or  $b$  small but  $d$  large as model II in Fig. 5(b) shows for this section. The linearly increasing modulation and the small value of  $a$  in model I or increasing modulation plus small  $c$  in model II causes the catch-up process in the section on the left to be relatively weak for both models.

**4.2 Optimal Non-Reciprocity.** Numerical simulations were performed to test for non-reciprocal transmission. All results presented in this section are obtained using the parameters of Table 1 with totally 100 bilinear springs.

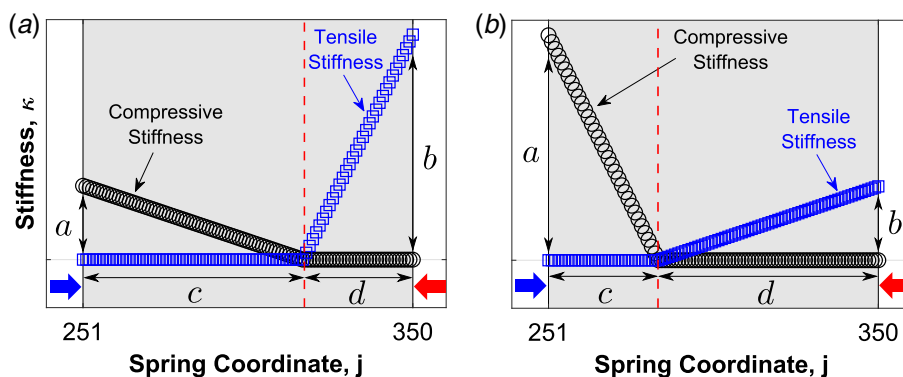


Fig. 5 Asymmetric stiffness-location modulation models. The dashed line separates the bilinear chain into two parts. On the left-hand side,  $a$  is the maximum difference between the stiffness of a bilinear spring in compression and in tension, and  $c$  is the number of the bilinear springs in this part. On the right-hand side,  $b$  is the maximum stiffness difference, and  $d$  is the number of bilinear springs. For model I, we have  $a < b$  and  $c > d$ ;  $a > b$  and  $c < d$  for model II. In subsequent simulations, the blue and red arrows are used to indicate the opposite pulse propagation directions: blue for incidence from the left and red from the right. (a) Modulation model I. (b) Modulation model II. (Color version online.)

**Table 2 Parameters for the non-reciprocal models of Fig. 5, using Eq. (12), to calculate the bilinear stiffness increments**

	$a$	$b$	$c$	$d$
Model I	1	1–10	67	33
Model II	1–10	1	33	67

Note: For model I,  $a$ ,  $c$ , and  $d$  are fixed and only  $b$  changes; for model II, we set  $b$ ,  $c$ , and  $d$  constant and vary only  $a$ .

We start with model I in Fig. 5(a) for an incident CT pulse. We fix the values of  $a$ ,  $c$ , and  $d$  listed in Table 2 and vary the value of  $b$  only. Figures 6(a) and 6(c) show the transmitted pulse amplitudes for different values of  $b/a$ . The incident pulse from the left first shows an effective increase in the distance between compressive and tensile zones in the section on the left. Then, the slow catch-up decreases the pulse amplitude in the section on the right. We therefore expect a CT pulse with diminished amplitude after transmission as shown in Fig. 6(a). Conversely, the same pulse propagating from the right first has an effective catch-up in the right section, which results in a change of pulse type. In the left section, the second catch-up process evolves slowly. We therefore expect a TC pulse if no pulse-type change occurs, e.g., cases  $b/a = 6, 8, 10$  in Fig. 6(c), or the existence of both pulse types such as case  $b/a = 4$ , or a CT pulse with the smaller amplitude if the fully second pulse-type change happens like case  $b/a = 2$ . Most importantly, the amplitudes of the transmitted waves from the opposite directions are of different orders of magnitude, as evident from Figs. 6(a) and 6(c), demonstrating significant non-reciprocal transmission.

Transmission from the opposite incidence directions is quantified by calculating the amplitude ratios of the transmitted and incident pulses based on the data in Fig. 6. These demonstrate significant wave non-reciprocity. Figure 7(a) shows results for all  $b/a$  cases.

Since the transmitted envelope (transmitted results for incidence from the right) consists of two types of pulses, we only take one of the greater absolute value into consideration. Here, we consider fully non-reciprocal or one-way propagation to be approximately achieved when the absolute amplitude ratio in Fig. 7(a) is less than 10%. To find the value of  $b/a$  that satisfies this almost-zero transmission condition, we introduce a box to Fig. 7(a). The upper and lower edges of the box, respectively, indicate the 10% and 0% amplitude ratios, and left and right edges give us the boundaries of the  $b/a$  range. Since the pulse propagation from the right results in almost zero transmission but the transmitted pulse from the left remains significant in amplitude, and the difference between the amplitude ratios for the opposite propagation direction is about one order of magnitude, we conclude that essentially one-way propagation can be realized using model I.

Next, model II in Fig. 5(b) is considered with only the value of  $a$  varied, and the ratio  $a/b$  is used as the indicator for different tests; the values of  $b$ ,  $c$ , and  $d$  are listed in Table 2. The CT pulse goes through the exactly same process as we described in the first model. Figures 6(b) and 6(d) show the transmitted pulse amplitudes from the opposite directions for various values of  $a/b$ , demonstrating evident non-reciprocal transmission. In Fig. 7(b), we find a broader parameter range that gives almost-zero transmission in model II, as compared with model I. As a result, one-way propagation can be realized in model II over a wide range of parameters, allowing tuning of the transmitted pulse.

Finally, we consider the non-reciprocal effect from the perspective of total incident and transmitted energy, kinetic plus potential. We calculate the input energy after the external forcing is fully applied; the transmitted energy is measured after the transmitted pulse has fully entered the linear part of the chain system as shown in Fig. 6. The velocities of the masses yield the kinetic energy and the relative displacements between adjacent masses define the potential energy. We focus on the non-dimensional ratio of transmitted to incident

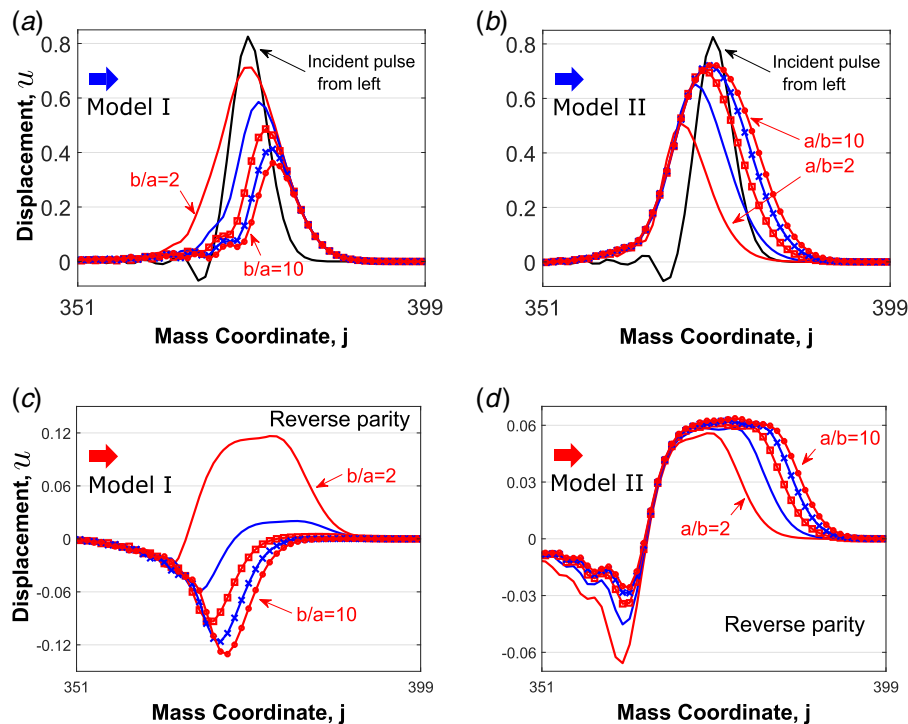


**Fig. 6** Transmitted amplitudes for the two models in Fig. 5: (a) and (c) model I on the left and (b) and (d) model II on the right. The curve indicated in (a) and (b) is the incident CT pulse; other curves represent the transmitted waves. Transmitted results for incidence from the left for model I are in (a) and from the right in (c), in both cases for  $b/a = 2, 4, 6, 8, 10$ , demonstrating very significant non-reciprocal transmission; similar phenomena are evident in (b), the results of incidence from the left, and (d), incidence from the right, which consider  $a/b = 2, 4, 6, 8, 10$  for model II.

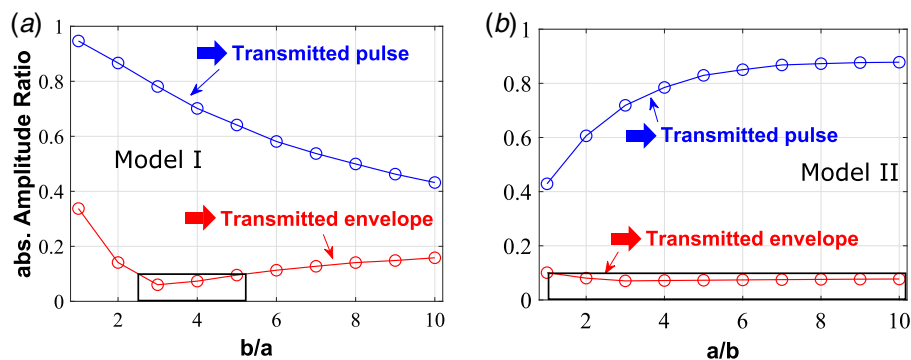


**Fig. 7** Transmission ratios for the two models in Fig. 5. The transmission is quantified by measuring the amplitude ratios of the transmitted and incident pulses based on the data in Fig. 6. The upper plots in (a) and (b) denote the ratios of incidence from the left, and the lower plots show the incidence from the right. Pulses maintain the same type (CT) before and after transmission for incidence from the left; the transmitted envelopes consist of CT and TC pulse for incidence from the right and we pick one of the greater absolute value for calculation. We consider that almost-zero transmission occurs when the absolute amplitude ratio is less than 10%. The boxes indicate the range of  $b/a$  and  $a/b$  values that satisfy the almost-zero transmission condition. Model II has a broader parameter range for one-way propagation.

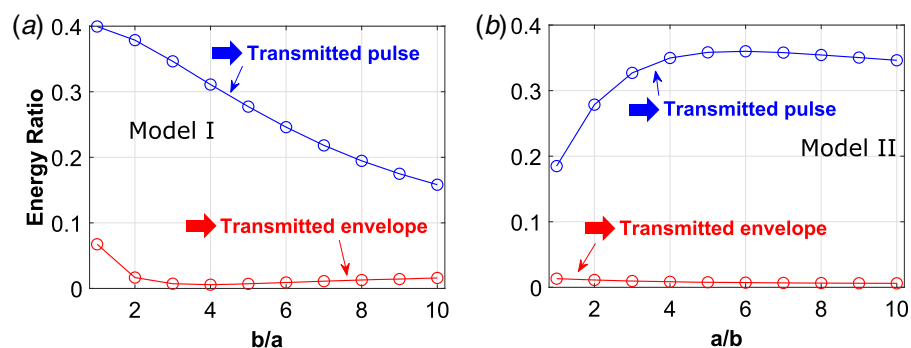


**Fig. 8** Transmitted energy ratios for the two models in Fig. 5. The upper plots in (a) and (b) denote the ratios of incidence from the left, and the lower plots show the incidence from the right. The values of  $b/a$  and  $a/b$  which satisfy the almost-zero transmission condition in Fig. 7 also produce significant non-reciprocal energy transmission.

energy. Figure 8(a) shows the energy ratios for various  $b/a$  values in model I. Comparison with the results in Fig. 7(a) shows that both absolute amplitude ratios and energy ratios show similar tendencies as functions of  $b/a$ . This phenomenon is also found in Fig. 8(b) which depicts all  $a/b$  cases in model II. Therefore,  $b/a$  and  $a/b$  values which

satisfy the almost-zero transmission condition from the amplitude perspective also produce significantly low transmitted energy. Furthermore, we find that a considerable amount of the incident energy is lost in transmission, over half as Fig. 8 shows. The remaining energy is mainly reflected with a small amount lost from damping.

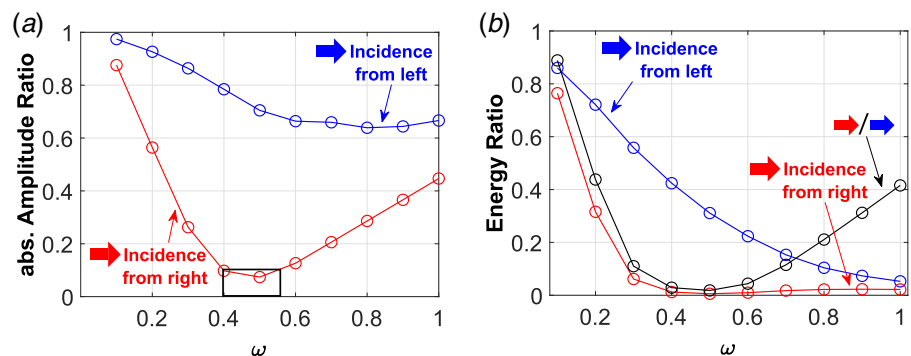


**Fig. 9** Transmission as a function of frequency for model I with  $b/a = 4$  from amplitude and energy perspectives: (a) transmitted amplitude and (b) transmitted energy. The box in (a) indicates the frequency range for almost-zero transmission according to its definition (ratio  $< 10\%$ ). The additional curve in (b) is the ratio of the transmitted energy for incidence from the right versus left.

**Table 3 The model parameter  $b/a$  and corresponding transmission ratios when the non-reciprocal wave motion occurs for different values of the incident pulse frequency  $\omega$**

$\omega$	$b/a$	$A_L$	$A_{R/L}$	$E_L$	$E_{R/L}$
0.3	10	0.660	0.126	0.407	0.033
0.4	6	0.672	0.099	0.356	0.024
0.6	2	0.825	0.088	0.311	0.025
0.7	1.5	0.876	0.110	0.207	0.051
0.8	1.2	0.757	0.146	0.147	0.095

Note:  $A_L$  and  $E_L$  are the amplitude and energy magnitudes from the left, relative to incident values.  $A_{R/L}$  and  $E_{R/L}$  represent ratios for incidence from the right versus left.

Only the CT incident pulse has been considered in this section. Non-reciprocal wave behavior is also found for TC input pulses, with details given in Appendix E.

#### 4.3 The Effect of Incident Frequency on Non-Reciprocity.

Here, we consider non-reciprocal transmission for a given model

optimized with constant value of incident frequency  $\omega$  and examine how it behaves for different frequencies.

Significant non-reciprocity was found in Sec. 4.2 for the case  $b/a = 4$ , based on the results in Figs. 7(a) and 8(a). We therefore focus on model I with fixed  $b/a = 4$  and examine what happens as  $\omega$  is varied. Figure 9(a) shows that the transmitted amplitude is strongly dependent on the incident frequency. The almost-zero transmission condition (absolute amplitude ratio  $<10\%$ ) can only be satisfied over a relatively small frequency range around  $\omega = 0.5$ , as the box in Fig. 9(a) shows. The behavior of the right-to-left transmitted energy ratio in Fig. 9(b), is consistent with this conclusion. These limited parameter studies suggest that the bilinear non-reciprocity effect is a relatively narrow band phenomenon.

However, for any given input forcing frequency  $\omega$ , there is always a model (a set of parameters) giving significant non-reciprocal transmission. We consider non-dimensional frequency  $\omega$  from 0.3 to 0.8 for model I and vary the parameter  $b/a$  (the rest of the parameters remain the same as in Table 2) to obtain optimal non-reciprocity. Table 3 shows the parameter  $b/a$  and corresponding transmission ratios when significant non-reciprocal propagation occurs. We note that all absolute amplitude ratios ( $A_{R/L}$ ) in this table are less than 15% and all energy ratios ( $E_{R/L}$ ) are less than 1%.

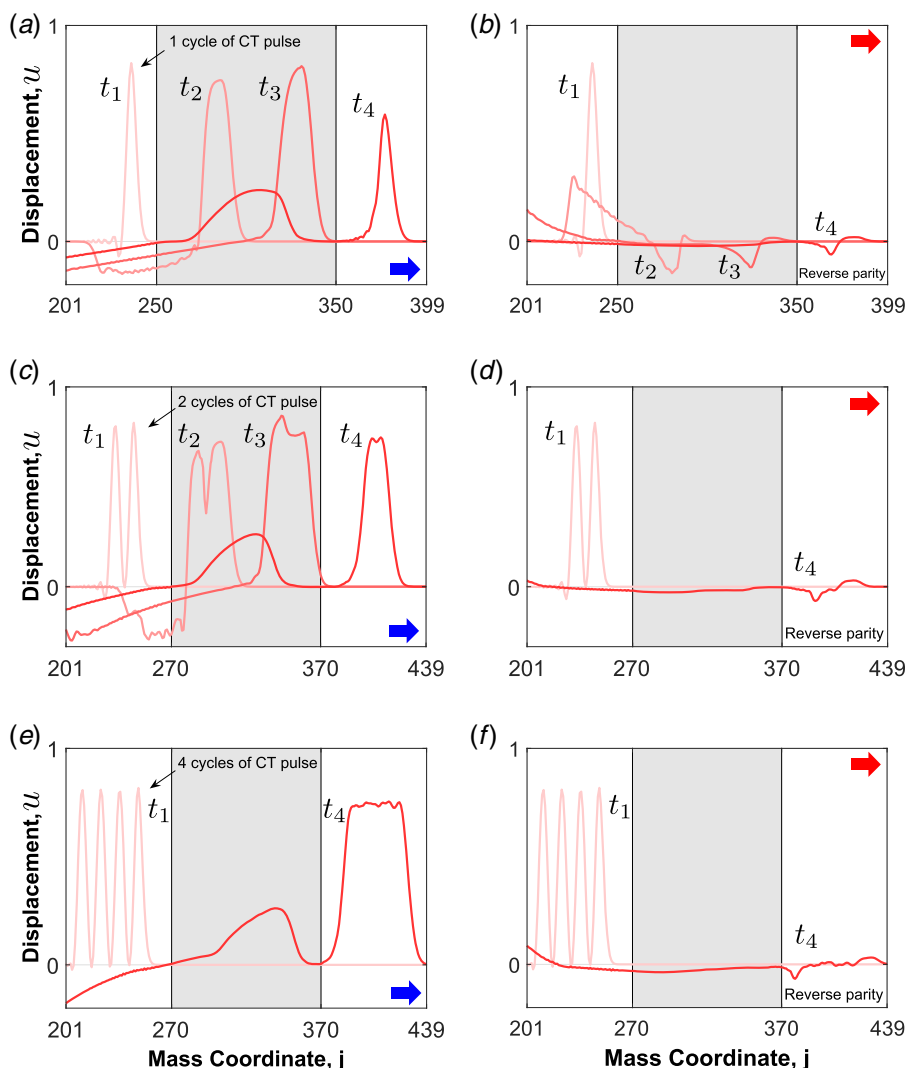


**Fig. 10 Dynamic properties of model I with  $b/a = 4$  when the incident wave consists of multiple cycles of a CT pulse. The plots on the left (right) correspond to incidence from the left (right). From the perspective of total energy, we find that  $E_L = 0.180$  and  $E_{R/L} = 0.019$  for (c) and (d); and for (e) and (f),  $E_L = 0.112$  and  $E_{R/L} = 0.019$ .**



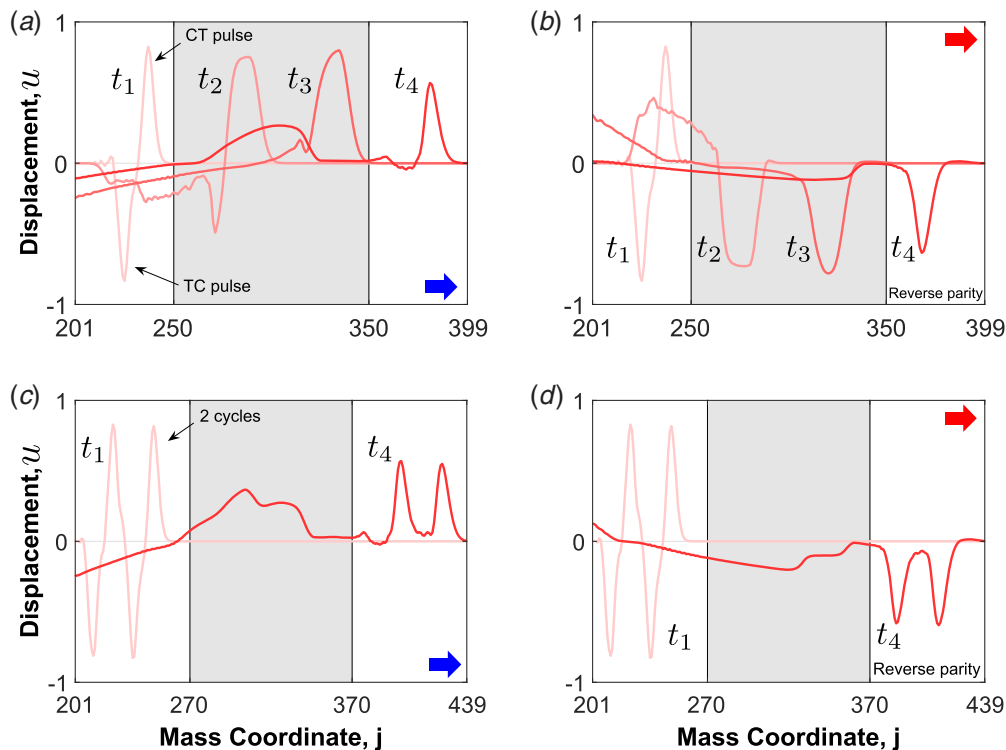


**Fig. 11 Dynamic properties of model I for an incident wave consisting of both pulse types. The plots on the left (right) correspond to incidence from the left (right). The incident wave in (a) and (b) corresponds to the forcing (Eq. (14)).**

**4.4 Propagation of Different Types of Incident Wave.** Our design of the non-reciprocal bilinear system is based on a single cycle of a CT or TC pulse. Here, we explore more general scenarios where the incident wave either consists of several cycles of a single pulse type or is a combination of both pulse types. We consider model I with  $b/a = 4$  for testing (see Fig. 5(a), with the other parameters as the same in Table 2).

Significant non-reciprocal wave motion is still observed if the incident wave consists of several cycles of a single pulse type, CT or TC. Figure 10 shows the dynamic response of model I for an incident wave consisting of  $n$  cycles of a CT pulse, for  $n = 1, 2$  and 4, corresponding to the forcing (obtained according to Eq. (5))

$$f = f_0 \mathcal{H}(t) \mathcal{H}\left(\frac{2n\pi}{\omega} - t\right) \sin \omega t \quad (13)$$

In each case of the wave with multiple cycles incident from the left, it is observed that the transmitted wave is a single cycle but extended in space and time. This characteristic shape is due to an approximate zero deformation zone in the transmitted wave. Conversely, a multiple cycle wave incident from the right produces a very low amplitude transmitted wave.

Finally, we consider an incident wave that contains both CT and TC pulse types. The forcing

$$f = f_0 \mathcal{H}(t) \mathcal{H}\left(\frac{2\pi}{\omega} - t\right) \sin \omega t - f_0 \mathcal{H}\left(t - \frac{2\pi}{\omega}\right) \mathcal{H}\left(\frac{4\pi}{\omega} - t\right) \sin \omega t \quad (14)$$

produces the incident wave in Figs. 11(a) and 11(b), which is a CT pulse followed by a TC pulse. The incident wave in Figs. 11(c) and 11(d) is two cycles of the CT/TC pulse. In both cases, Fig. 11 shows that there is always a non-zero transmitted pulse of either CT or TC type, with the pulse type dependent on the incidence direction.

Thus, incidence from the left (right) produces a transmitted wave that is purely of CT (TC) type. This phenomenon can be understood by recalling Fig. 6 for CT incidence and Fig. 15 in Appendix E for TC incidence. When a wave consisting of both pulse types propagates from one side, one of them results in zero transmission (e.g., TC input pulse propagates from left in model I, as Fig. 15(a) shows) and the other a transmitted pulse with type unchanged and amplitude slightly decreased (e.g., CT input pulse propagates from left in model I, as Fig. 6(a) shows). In sum, the transmission is purely CT or TC for incidence from the left or right, respectively. This filtering effect is strongly non-reciprocal.

## 5 Conclusion

We have demonstrated a passive 1D spring-mass-damper chain structure that breaks elastic wave reciprocity. Amplitude-independent non-reciprocity is a result of introducing bilinear springs and carefully designing the spatially inhomogeneous and asymmetric modulations of the bilinear stiffness. A compression-tension pulse is used to quantify non-reciprocal transmission. Incident pulses from opposite directions result in significantly different transmitted pulses; almost-zero transmission with significant transmission from the other direction has been demonstrated. The results shown here indicate that a simple 1D bilinear chain system can produce non-reciprocal wave dynamics and is therefore suited for a variety of elastic wave control mechanisms, such as one-way propagation, pulse-type inversion, pulse-type filtering, etc. Moreover, these simple models can work as the building blocks for some more complex, higher dimensional non-reciprocal structure designs.

## Acknowledgment

This work is supported by the NSF EFRI program under Award No. 1641078.

## Appendix A: Stiffness and Damping Coefficients in the Perfectly Matched Layer

A PML is attached to the test chain at each end to eliminate reflections, see Fig. 1. Suppose that the index  $j$  starts from 1 at the beginning of the PML on the left. Each PML is a linear spring-mass-damper chain in which the damping coefficients are “ramped-up” to avoid internal reflections. The location-dependent parameters of the left and right PMLs are symmetric about the central test chain. Here, we concentrate on the PML on the left in which the dimensionless stiffness is  $\kappa_j = 1$ . The PML index takes the values  $1 \leq j \leq N_{pml}$ , with dimensionless damping coefficient

$$\zeta_j = \zeta_{\max} \left( \frac{N_{pml} + 1 - j}{N_{pml}} \right)^3 \quad (A1)$$

where  $\zeta_{\max}$  is the maximum damping coefficient of the PML. All the numerical experiments take  $\zeta_{\max} = 10$ .

## Appendix B: The Effect of Damping in the Bilinear Chain

We include damping in the bilinear section in order to understand how any realistic damping affects wave propagation. Figure 12 compares cases with and without damping. We find that the weak dampers in the bilinear chain do not significantly affect the propagation results in terms of the pulse shape and size. Shock-like wave structures can be observed in Fig. 12(a). Damping has a strong smoothing effect as can be seen in Figs. 12(b) and 12(c). In particular, Fig. 12(c) shows a clear pulse shape with the characteristic feature of a zero deformation zone. For this reason, we choose to set dimensionless damping coefficient  $\zeta_0 = 0.1$  for numerical simulations in this paper.

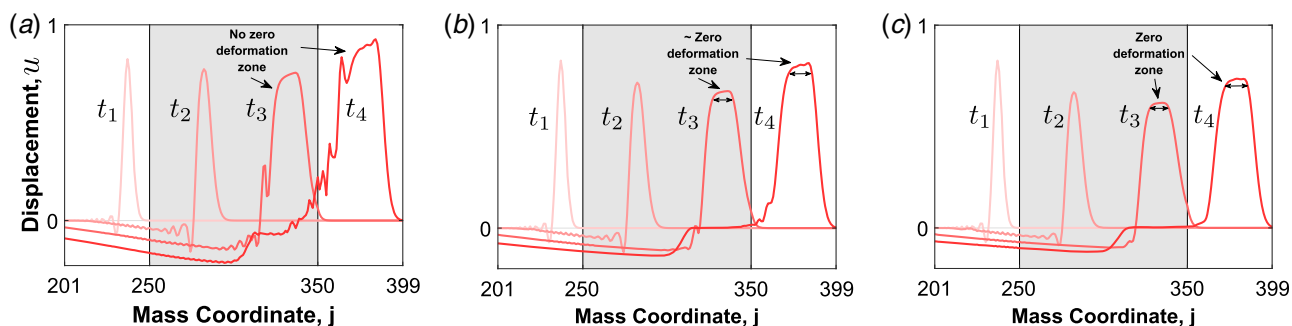


Fig. 12 A comparison of the response with and without damping in the bilinear section. (a) The displacement fields at different instants for the modulation of Fig. 3(a) without damping, (b) and (c) with constant weak damping ( $\zeta_0 = 0.05$  and  $0.1$ , respectively).

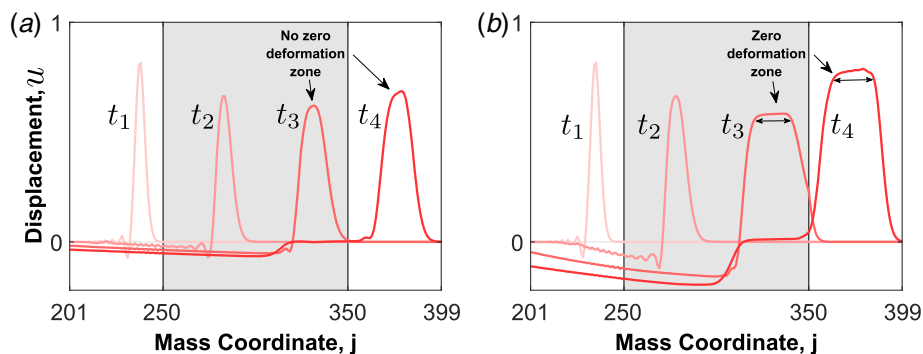


Fig. 13 The effect of the stiffness modulation slope in Fig. 3(a) on the length of the zero deformation zone. Zero deformation is barely observed in (a). However, as compared with Fig. 3(c), (b) indicates that the greater slope leads to a significantly longer zero deformation regime. (a) Slope =  $0.5/100$  and (b) Slope =  $2/100$ .

## Appendix C: Spatial Modulation of the Bilinear Stiffness

The fundamental modulations in Sec. 3 are designed based on the rule of spatial inhomogeneity and asymmetry, necessary but not sufficient for achieving wave non-reciprocity. Spatial inhomogeneity and asymmetry are obtained by a linear modulation of the stiffness. Figure 13 shows how the slope of the stiffness curve affects transmission, in this case through the length of the zero deformation regime. The reason is that larger values of  $\Delta_{j,c}$  increase the slope of the stiffness curve, leading to greater compressive wave speeds, which in turn results in larger sizes of the zero deformation zone.

A TC pulse is used for testing the different configurations, generated using the negative sign in the external loading (Eq. (5)). Assuming that the stiffness of the bilinear spring is greater in compression than in tension, we set  $\Delta_{j,c} > \Delta_{j,t} = 0$  and  $\Delta_{j,c}$  changes linearly over location according to Eqs. (8) and (9). Figures 14(a) and 14(b) depict the displacement fields along the test chain at four different moments for the stiffness modulations of Figs. 3(a) and 3(b), respectively. Conversely, when the bilinear spring has a greater stiffness in tension than compression:  $\Delta_{j,t} > \Delta_{j,c} = 0$  where  $\Delta_{j,t}$  changes linearly according to Eqs. (10) and (11), the displacement fields for the modulation of Figs. 4(a) and 4(b) are shown in Figs. 14(c) and 14(d), respectively.

## Appendix D: Dimensionless Stiffness for Incidence From the Right

Two asymmetric stiffness-location modulation models for breaking wave reciprocity are considered, as shown in Fig. 5. The designs are based on the fundamental asymmetric nonlinear configurations in Sec. 3. For pulse propagation from the right (as the red arrow indicates), the index  $j$  starts from 1 at the right end of the test

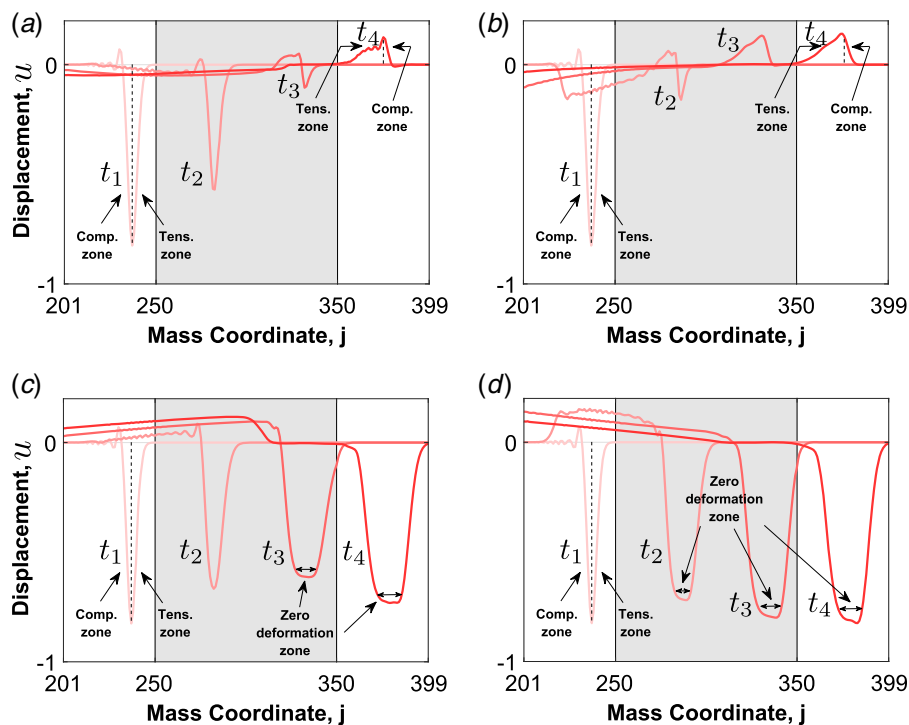


**Fig. 14** Dynamic properties of the bilinear spring chain. (a) and (b) The displacement fields of the bilinear chain at four different moments for modulations given by Figs. 3(a) and 3(b), respectively. (c) and (d) The displacement fields for modulations shown in Figs. 4(a) and 4(b), respectively.

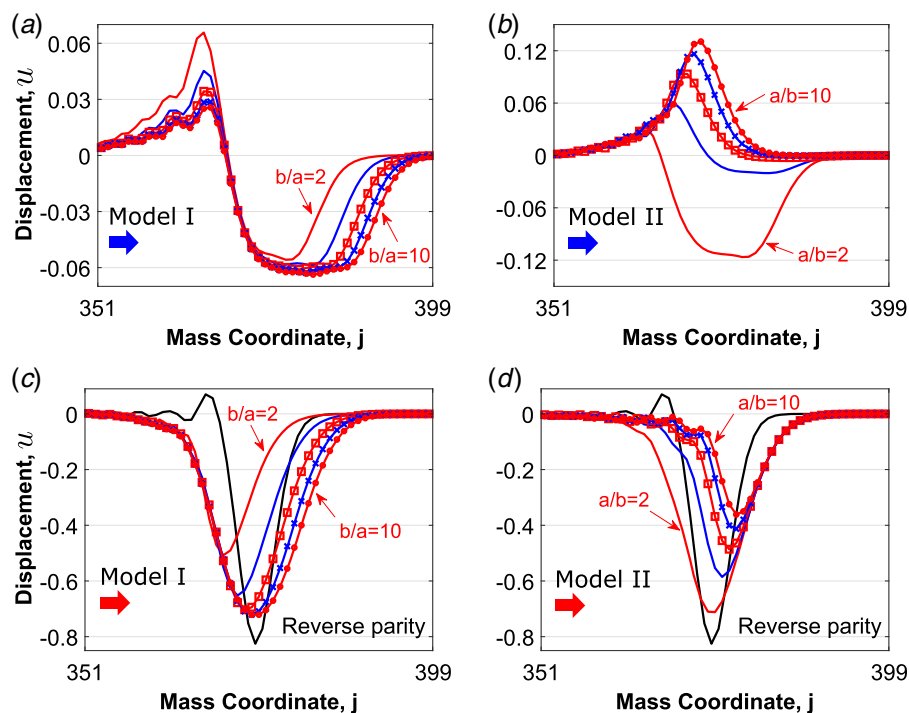


**Fig. 15** Transmitted amplitudes for the two models in Fig. 5 with a TC input pulse: (a) and (c) model I on the left and (b) and (d) model II on the right. The curve with the largest pulse amplitude in (c) and (d) is the incident TC pulse; other curves represent the transmitted waves. Incidence from the left for model I is in (a) and from the right in (c), in both cases for  $b/a = 2, 4, 6, 8, 10$ , demonstrating very significant non-reciprocal transmission; similar phenomena are evident in (b), the results of incidence from the left, and (d), incidence from the right, which consider  $a/b = 2, 4, 6, 8, 10$  for model II.

**Table 4 The relation between the simulation results of the cases using CT pulse in Fig. 6 and TC pulse in Fig. 15**

	Model I (L)	Model I (R)	Model II (L)	Model II (R)
CT pulse	Fig. 6(a)	Fig. 6(c)	Fig. 6(b)	Fig. 6(d)
TC pulse	Fig. 15(a) = -Fig. 6(d)	Fig. 15(c) = -Fig. 6(b)	Fig. 15(b) = -Fig. 6(c)	Fig. 15(d) = -Fig. 6(a)

Note:  $L$  and  $R$  represent the case of incidence from the left and right, respectively. The negative sign in the second row denotes sign inversion of the displacements.

chain in Fig. 1 (reverse parity) and takes the value  $N_l + 1 < j \leq N_l + 1 + d(N_{bl} - 1)/(c + d)$  for the right section of the bilinear part and  $N_l + 1 + d(N_{bl} - 1)/(c + d) < j \leq N_l + N_{bl}$  for the left. The dimensionless stiffness increments  $\Delta_{j,c}$  and  $\Delta_{j,t}$  are

$$\Delta_{j,c} = \begin{cases} 0 & \text{right section} \\ a \frac{j - N_l - 1 - \frac{d}{c+d}(N_{bl} - 1)}{\frac{c}{c+d}(N_{bl} - 1)} & \text{left section} \end{cases} \quad (D1)$$

$$\Delta_{j,t} = \begin{cases} b \frac{N_l + 2 + \frac{d}{c+d}(N_{bl} - 1) - j}{\frac{d}{c+d}(N_{bl} - 1)} & \text{right section} \\ 0 & \text{left section} \end{cases}$$

## Appendix E: Propagation of a Tension–Compression Input Pulse

A CT incident pulse is considered in Sec. 4 for demonstrating non-reciprocal wave effects. In the same way, it is able to realize non-reciprocal wave behavior when the input pulse is TC type, as shown in Fig. 15. Figures 15(a) and 15(c) show the transmitted pulse amplitudes for different  $b/a$  values in model I. These results are equivalent to sign inversion of the data presented in Figs. 6(d) and 6(b), which are the results for CT pulse incidence. The same phenomenon can be found in model II. Table 4 summarizes the relationship between the simulation results using the two different incident pulse types.

## References

- [1] Caloz, C., Alù, A., Tretyakov, S., Sounas, D., Achouri, K., and Deck-Léger, Z.-L., 2018, "Electromagnetic Nonreciprocity," *Phys. Rev. Appl.*, **10**(4), p. 047001.
- [2] Wang, P., Lu, L., and Bertoldi, K., 2015, "Topological Phononic Crystals With One-Way Elastic Edge Waves," *Phys. Rev. Lett.*, **115**(10), p. 104302.
- [3] Nassar, H., Xu, X., Norris, A., and Huang, G., 2017, "Modulated Phononic Crystals: Non-Reciprocal Wave Propagation and Willis Materials," *J. Mech. Phys. Solids*, **101**(C), pp. 10–29.
- [4] Nassar, H., Chen, H., Norris, A. N., and Huang, G. L., 2018, "Quantization of Band Tilting in Modulated Phononic Crystals," *Phys. Rev. B*, **97**(1), p. 014305.
- [5] Liang, B., Yuan, B., and Cheng, J.-C., 2009, "Acoustic Diode: Rectification of Acoustic Energy Flux in One-Dimensional Systems," *Phys. Rev. Lett.*, **103**(10), p. 104301.
- [6] Liang, B., Guo, X. S., Tu, J., Zhang, D., and Cheng, J. C., 2010, "An Acoustic Rectifier," *Nat. Mater.*, **9**(12), pp. 989–992.
- [7] Fronk, M. D., Tawfik, S., Daraio, C., Li, S., Vakakis, A., and Leamy, M. J., 2019, "Acoustic Non-Reciprocity in Lattices With Nonlinearity, Internal Hierarchy, and Asymmetry: Computational Study," *ASME J. Vib. Acoust.*, **141**(5), p. 051011.
- [8] Moore, K. J., Bunyan, J., Tawfik, S., Gendelman, O. V., Li, S., Leamy, M., and Vakakis, A. F., 2018, "Nonreciprocity in the Dynamics of Coupled Oscillators With Nonlinearity, Asymmetry, and Scale Hierarchy," *Phys. Rev. E*, **97**(1), p. 012219.
- [9] Bunyan, J., Moore, K. J., Mojahed, A., Fronk, M. D., Leamy, M., Tawfik, S., and Vakakis, A. F., 2018, "Acoustic Nonreciprocity in a Lattice Incorporating Nonlinearity, Asymmetry, and Internal Scale Hierarchy: Experimental Study," *Phys. Rev. E*, **97**(5), p. 052211.
- [10] Luo, B., Gao, S., Liu, J., Mao, Y., Li, Y., and Liu, X., 2018, "Non-Reciprocal Wave Propagation in One-Dimensional Nonlinear Periodic Structures," *AIP Adv.*, **8**(1), p. 015113.
- [11] Wallen, S. P., and Haberman, M. R., 2019, "Nonreciprocal Wave Phenomena in Spring-Mass Chains With Effective Stiffness Modulation Induced by Geometric Nonlinearity," *Phys. Rev. E*, **99**(1), p. 013001.
- [12] Narisetti, R. K., Leamy, M. J., and Ruzzene, M., 2010, "A Perturbation Approach for Predicting Wave Propagation in One-Dimensional Nonlinear Periodic Structures," *ASME J. Vib. Acoust.*, **132**(3), p. 031001.
- [13] Narisetti, R. K., Ruzzene, M., and Leamy, M. J., 2012, "Study of Wave Propagation in Strongly Nonlinear Periodic Lattices Using a Harmonic Balance Approach," *Wave Motion*, **49**(2), pp. 394–410.
- [14] Shaw, S., and Holmes, P., 1983, "A Periodically Forced Piecewise Linear Oscillator," *J. Sound Vib.*, **90**(1), pp. 129–155.
- [15] Scalerandi, M., Agostini, V., Delsanto, P. P., Abeele, K. V. D., and Johnson, P. A., 2003, "Local Interaction Simulation Approach to Modelling Nonclassical, Nonlinear Elastic Behavior in Solids," *J. Acoust. Soc. Am.*, **113**(6), p. 3049.
- [16] Kuznetsova, M. S., Pasternak, E., and Dyskin, A. V., 2017, "Analysis of Wave Propagation in a Discrete Chain of Bilinear Oscillators," *Nonlinear Processes Geophys.*, **24**(3), pp. 455–460.
- [17] Benveniste, Y., 1980, "One-Dimensional Wave Propagation in Materials With Different Moduli in Tension and Compression," *Int. J. Eng. Sci.*, **18**(6), pp. 815–827.
- [18] Maslov, V., and Mosolov, P., 1985, "General Theory of the Solutions of the Equations of Motion of an Elastic Medium of Different Moduli," *J. Appl. Math. Mech.*, **49**(3), pp. 322–336.
- [19] Nazarov, V. E., and Ostrovsky, L. A., 1990, "Elastic Waves in Media With Strong Acoustic Nonlinearity," *Sov. Phys. Acoust.*, **36**(1), pp. 106–110.
- [20] Ostrovsky, L. A., 1991, "Wave Processes in Media With Strong Acoustic Nonlinearity," *J. Acoust. Soc. Am.*, **90**(6), pp. 3332–3337.
- [21] Abeyaratne, R., and Knowles, J. K., 1992, "Wave Propagation in Linear, Bilinear and Trilinear Elastic Bars," *Wave Motion*, **15**(1), pp. 77–92.
- [22] Gavrilov, S., and Herman, G., 2012, "Wave Propagation in a Semi-Infinite Heteromodal Elastic Bar Subjected to a Harmonic Loading," *J. Sound Vib.*, **331**(20), pp. 4464–4480.
- [23] Nazarov, V. E., Radostin, A. V., and Kiyashko, S. B., 2015, "Self-Similar Acoustic Waves in Homogeneous Media With Different-Modulus Nonlinearity and Relaxation," *Radiophys. Quantum Electron.*, **58**(2), pp. 124–131.
- [24] Rudenko, O. V., 2016, "Modular Solitons," *Dokl. Math.*, **94**(3), pp. 708–711.
- [25] Rudenko, O. V., 2016, "Equation Admitting Linearization and Describing Waves in Dissipative Media With Modular, Quadratic, and Quadratically Cubic Nonlinearities," *Dokl. Math.*, **94**(3), pp. 703–707.
- [26] Nazarov, V. E., Kiyashko, S. B., and Radostin, A. V., 2016, "The Wave Processes in Micro-Inhomogeneous Media With Different-Modulus Nonlinearity and Relaxation," *Radiophys. Quantum Electron.*, **59**(3), pp. 246–256.
- [27] Naugolnykh, K., and Ostrovsky, L., 1998, *Nonlinear Wave Processes in Acoustics*, Cambridge University Press, Cambridge.